

Trends in Austral jet position in ensembles of high- and low-top CMIP5 models

Article

Published Version

Wilcox, L. J. ORCID: <https://orcid.org/0000-0001-5691-1493>, Charlton-Perez, A. J. ORCID: <https://orcid.org/0000-0001-8179-6220> and Gray, L. J. (2012) Trends in Austral jet position in ensembles of high- and low-top CMIP5 models. *Journal of Geophysical Research - Atmospheres*, 117. D13115. ISSN 0148-0227 doi: <https://doi.org/10.1029/2012JD017597>
Available at <https://centaur.reading.ac.uk/28494/>

It is advisable to refer to the publisher's version if you intend to cite from the work. See [Guidance on citing](#).

Published version at: <http://www.agu.org/pubs/crossref/2012/2012JD017597.shtml>

To link to this article DOI: <http://dx.doi.org/10.1029/2012JD017597>

Publisher: American Geophysical Union

All outputs in CentAUR are protected by Intellectual Property Rights law, including copyright law. Copyright and IPR is retained by the creators or other copyright holders. Terms and conditions for use of this material are defined in the [End User Agreement](#).

www.reading.ac.uk/centaur

CentAUR

Central Archive at the University of Reading

Reading's research outputs online

Trends in Austral jet position in ensembles of high- and low-top CMIP5 models

L. J. Wilcox,^{1,2} A. J. Charlton-Perez,² and L. J. Gray^{1,3}

Received 8 February 2012; revised 27 April 2012; accepted 30 May 2012; published 13 July 2012.

[1] Trends in the position of the DJF Austral jet have been analyzed for multimodel ensemble simulations of a subset of high- and low-top models for the periods 1960–2000, 2000–2050, and 2050–2098 under the CMIP5 historical, RCP4.5, and RCP8.5 scenarios. Comparison with ERA-Interim, CFSR and the NCEP/NCAR reanalysis shows that the DJF and annual mean jet positions in CMIP5 models are equatorward of reanalyses for the 1979–2006 mean. Under the RCP8.5 scenario, the mean jet position in the high-top models moves 3 degrees poleward of its 1860–1900 position by 2098, compared to just over 2 degrees for the low-top models. Changes in jet position are linked to changes in the meridional temperature gradient. Compared to low-top models, the high-top models predict greater warming in the tropical upper troposphere due to increased greenhouse gases for all periods considered: up to 0.28 K/decade more in the period 2050–2098 under the RCP8.5 scenario. Larger polar lower-stratospheric cooling is seen in high-top models: –1.64 K/decade compared to –1.40 K/decade in the period 1960–2000, mainly in response to ozone depletion, and –0.41 K/decade compared to –0.12 K/decade in the period 2050–2098, mainly in response to increases in greenhouse gases. Analysis suggests that there may be a linear relationship between the trend in jet position and meridional temperature gradient, even under strong forcing. There were no clear indications of an approach to a geometric limit on the absolute magnitude of the poleward shift by 2100.

Citation: Wilcox, L. J., A. J. Charlton-Perez, and L. J. Gray (2012), Trends in Austral jet position in ensembles of high- and low-top CMIP5 models, *J. Geophys. Res.*, 117, D13115, doi:10.1029/2012JD017597.

1. Introduction

[2] The recent poleward shift of the extratropical Austral jet is well established. The shift in the surface westerlies is typically described as a trend in the Southern Annular Mode (SAM) toward its positive phase. Such trends are seen in radiosonde observations [Marshall, 2003]. Poleward shifts are also seen in the subtropical jet in observations (Hudson [2011], using ozone measurements; Fu and Lin [2011] using MSU data) and reanalyses [Archer and Caldeira, 2008], indicating an expansion of the tropical belt [Seidel *et al.*, 2008].

[3] The change in the position of the jet in the last three decades has been shown to be a response to the concomitant forcing from decreasing stratospheric ozone and increasing greenhouse gases (GHGs), with models unable to reproduce the shift without a representation of stratospheric ozone depletion [Son *et al.*, 2008]. Model studies, where responses

to increasing GHGs and changes in stratospheric ozone can be analyzed independently, have shown that the December to February mean (DJF) circulation changes seen to date in the Southern Hemisphere (SH) are driven primarily by stratospheric ozone depletion [Arblaster and Meehl, 2006; McLandress *et al.*, 2011a; Polyani *et al.*, 2011]. The primary role of stratospheric ozone depletion in driving Austral jet trends in recent decades suggests that a cancellation, or even reversal, of the poleward trends can be expected in the near future as ozone concentrations recover.

[4] In order to highlight the interaction between stratospheric ozone and GHG forcing on the Austral jet, this work focuses on the DJF circulation. Although the largest forcing from stratospheric ozone occurs from September to November, when the ozone hole is at its deepest, the largest tropospheric response is seen in DJF [Thompson and Solomon, 2002].

[5] The fifth Coupled Model Intercomparison Project (CMIP5) provides a unique opportunity to compare the response of several models to the same future scenarios, including a consistent ozone forcing scenario [Cionni *et al.*, 2011], which is used in all models that do not include interactive chemistry.

[6] The CMIP5 set of models also includes a substantial number of ‘high-top’ models, which explicitly resolve the stratosphere. This facilitates the first multimodel comparison of models with and without a fully resolved stratosphere. ‘Low-top’ models have been shown to have a cold bias in

¹NCAS-Climate, Reading, UK.

²Department of Meteorology, University of Reading, Reading, UK.

³Department of Atmospheric, Oceanic and Planetary Physics, University of Oxford, Oxford, UK.

Corresponding author: L. J. Wilcox, Department of Meteorology, University of Reading, Earley Gate, PO Box 243, Reading RG6 6BB, UK. (l.j.wilcox@reading.ac.uk)

©2012. American Geophysical Union. All Rights Reserved.
10.1029/2012JD017597

Table 1. CMIP5 Models Used in This Study^a

Model	Ensemble Members	nlon	nlat	nlevs	Horizontal Resolution	Model Top
CNRM-CM5	1	256	128	31	TL127	10 hPa
CSIRO-Mk3.6.0	1	192	96	18	T63	4.52 hPa
HadGEM2-ES	4	192	144	38	N96	40 km (~2.3 hPa)
INMCM4	1	180	120	21	180 × 120	10 hPa
MIROC5	1	256	128	40	T85	3 hPa
NCAR-CCSM4	1	288	192	27	0.9° × 1.25°	2.194 hPa
NorESM1-M	1	144	96	26	f19	3.54 hPa
CanESM2 ^b	5	128	64	35	T63	1 hPa
GFDL-CM3 ^b	1	144	90	48	C48	0.01 hPa
HadGEM2-CC ^b	1	192	144	60	N96	85 km (~0.01 hPa)
IPSL-CM5A-LR ^b	4	96	96	39	96 × 95	0.04 hPa
MIROC-ESM-CHEM ^b	1	128	64	80	T42	0.0036 hPa
MPI-ESM-LR ^b	1	192	96	47	T63	0.01 hPa
MRI-CGCM3 ^b	1	320	160	48	TL159	0.01 hPa

^aEnsemble members are consistent across all runs.

^bHigh top models.

the upper stratosphere, and to underestimate variability in the lower stratosphere [Cordero and Forster, 2006].

2. Data Sets

[7] The CMIP5 models used in this study, and their classification, are shown in Table 1. High-top models have been defined here as those with model tops at pressures ≤ 1 hPa, or altitudes ≥ 45 km. All model simulations include a representation of the major known climate forcings, including greenhouse gases, ozone, tropospheric aerosol, volcanic aerosol, and solar variations. Observed forcing is used in the historical period (1850–2005). In future scenarios, ozone is derived from a multimodel ensemble of coupled-chemistry models [Cionni *et al.*, 2011], which removes a degree of

uncertainty compared to CMIP3. Greenhouse gas future scenarios (2006–2100) follow the Representative Concentration Pathways (RCP) 4.5 [Thomson *et al.*, 2011], and RCP8.5 [Riahi *et al.*, 2011]. The two pathways result in a global-mean radiative forcing of 4.5 Wm^{-2} and 8.5 Wm^{-2} respectively by 2100, with RCP4.5 carbon dioxide emissions peaking around 2040, and RCP8.5 emissions peaking in 2100.

[8] Annual-mean global-mean GHG concentrations, and September–November Antarctic mean ($75\text{--}90^\circ\text{S}$) ozone concentration at 50 hPa, are shown in Figure 1. Ozone concentration begins slowly to decrease in the early 20th century, with a rapid decrease from 1970. The concentration has a minimum in 1997, and then increases almost linearly until 2065, when the rate of increase begins to slow. In

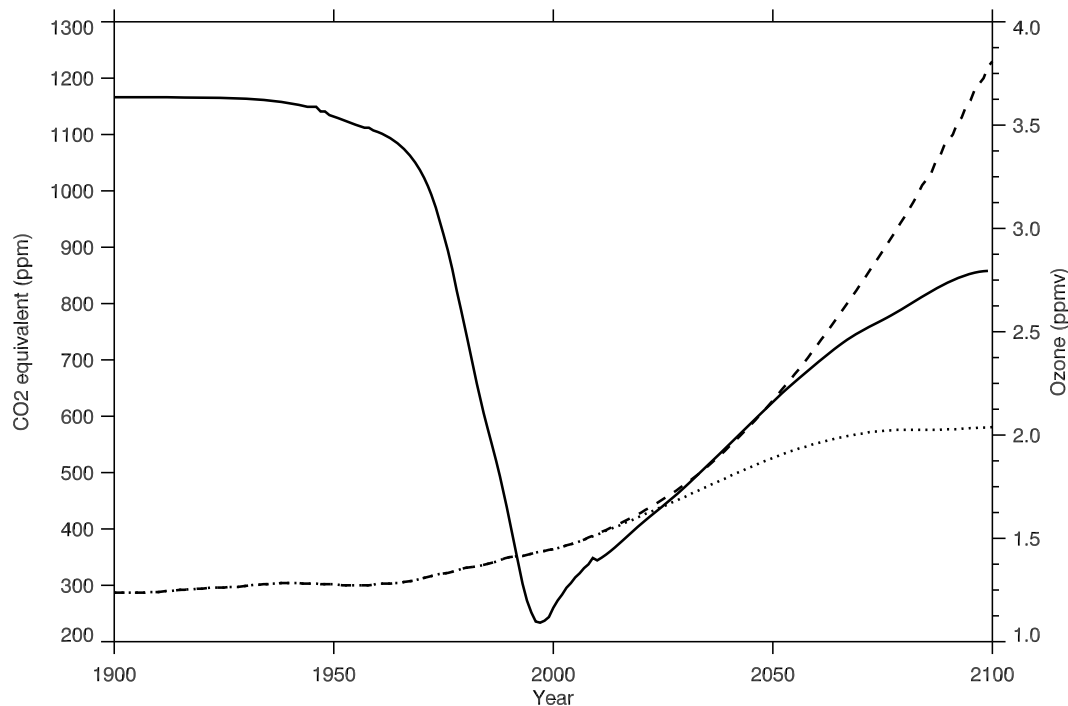


Figure 1. Annual average global mean greenhouse gas concentration (as CO_2 equivalent (ppm)) in RCP4.5 (dotted) and RCP8.5 (dashed), and September to October mean Antarctic ($75\text{--}90^\circ\text{S}$) ozone at 50 hPa (ppmv) (solid).

RCP8.5 GHG concentrations increase almost exponentially through the 21st century, while in RCP4.5 they increase at a similar rate to recent decades, before stabilizing in the last decades of the 21st century. In this study, we define three analysis periods, chosen to reflect the key features of these concentrations: 1960–2000 to capture ozone depletion; 2000–2050 to capture ozone recovery; and 2050–2100 as a period when there are large differences between RCP4.5 and RCP8.5, and when GHG forcing is likely to dominate over stratospheric ozone, which recovers to 1980 levels by 2070. Data availability for some models means that trends for this GHG dominated period can only be evaluated for 2050–2098.

[9] Trends in temperature and jet position are derived from monthly mean data. Different numbers of ensemble members are available for each of the models. Where multiple ensemble members are available for the historical, RCP4.5, and RCP8.5 runs, trend estimates are derived by first calculating the ensemble mean of the appropriate quantity; the ensemble mean is then used for that model. The number of ensemble members used for each model is shown in Table 1. Where multimodel means have been used, every model has been given equal weight.

[10] The ERA-Interim (1979–present) [Dee *et al.*, 2011], the NCEP/NCAR reanalysis (1948–present) [Kalnay *et al.*, 1996], and the new, higher horizontal resolution, NCEP Climate Forecast System Reanalysis (CFSR) [Saha *et al.*, 2010] were used to assess biases in the model data. Data analysis systems in the reanalyses have resolutions of T255 L60, T62 L28, and T382 L64 respectively, and were used in this work on $512^\circ \times 256^\circ \times 37$ levels, $144^\circ \times 73^\circ \times 17$ levels, and $144^\circ \times 73^\circ \times 37$ levels.

3. Zonal-Mean Wind and Temperature

[11] To illustrate the typical climatology and trends in the zonal-mean zonal-wind and temperature in CMIP5, distributions from the HadGEM2-ES model are shown in Figure 2. The 1860–1900 climatology is overlaid with the linear trends for the stratospheric ozone depletion period (1960–2000) (Figures 2a and 2b), ozone recovery period (2000–2050) (Figures 2c and 2d), and well-mixed GHG dominated period (2050–2098) (Figures 2e and 2f). Trends from all other models (not shown) have similar structures in the temperature and zonal-wind trends, and HadGEM2-ES is used as an example only. As is clear from subsequent figures, the magnitude of these trends can vary considerably between models, especially in the period 2000–2050.

[12] Trends in zonal-mean temperature indicate a warming troposphere, with enhanced warming in the tropical upper troposphere, and generalized cooling in the stratosphere associated with well-mixed GHGs in all periods (Figures 2a, 2c, and 2e). Stratospheric ozone depletion results in a strong cooling trend in the polar lower stratosphere, with a maximum at 150 hPa (Figure 2a), which is replicated in the majority of models (not shown). This region warms while ozone levels recover (Figure 2c).

[13] In 1960–2000 (Figure 2b) and 2050–2098 (Figure 2f) the dipole structure in the extratropical tropospheric zonal-wind trends, with increasing westerlies on the poleward flank of the jet, and decreasing westerlies in alignment with and equatorward of the jet core, indicate a poleward shift of

the jet. Positive zonal-wind trends on the poleward side of the jet extend upwards through the depth of the stratosphere.

[14] As stratospheric ozone recovers, from 2000–2050, there is localized warming in the polar lower stratosphere (Figure 2c). The warming over the pole is associated with negative zonal-wind trends in the same region (Figure 2d). These negative trends extend through the troposphere on the poleward side of the jet in HadGEM2-ES, indicating an equatorward movement of the jet in 2000–2050 (Figure 2d).

[15] The reversal of the dipole in zonal-wind trends, and hence the reversal of the direction of the migration of the jet (shown in Figure 2d for HadGEM2-ES), is also seen in INMCM4, GFDL-CM3, and MIROC-ESM-CHEM. In other models a cancellation between stratospheric ozone and GHG forcing occurs, and little trend is seen in the tropospheric zonal-winds (CNRM-CM5, MRI-CGCM3, and HadGEM2-CC). The remainder of the models show a weakening of the poleward trend in the jet compared to 1960–2000 in response to stratospheric ozone recovery. Time series analyses show that in some individual models there is a reversal of the poleward trend in the jet over shorter time periods in the early 21st century, but that this is not always large enough or sustained enough to result in a reversal of the 50-year trend like that seen in HadGEM2-ES in Figure 2d.

[16] The magnitudes of trends in both zonal-mean temperature and zonal-mean zonal-wind are typically larger in the high-top models than the low-top models. This is reflected in the ensemble mean regional temperature and jet position trends (Figure 3). Figure 3 shows the high- and low-top ensemble mean DJF mean tropical upper-tropospheric (250 hPa, 0–25°S) and polar lower-stratospheric temperature (150 hPa, 75–90°S) under historical and RCP4.5, and historical and RCP8.5, forcing. ERA-Interim values of the same quantities are also shown. Enhanced warming in the tropical upper-troposphere in high-top models compared to low-top models can be seen, especially in RCP8.5 (solid lines in Figure 3a), with the difference between the two ensemble means increasing steadily with time. Figure 3b shows that the polar stratosphere of the low-top models is colder than the high-top models throughout the whole period. Both sets of models have a cold temperature bias here, although this is much more pronounced in the low-top ensemble. A larger and more rapid cooling of the polar lower-stratosphere in the stratospheric ozone depletion period in high-top models compared to those with low-tops can also be seen. Cooling in this region is also evident under RCP8.5 in the high-top mean from 2050, while there is almost no change in the low-top temperature. This suggests a tendency for GHG forcing to have more of a cooling influence in the stratosphere in the high-top models. In the last decades of the 21st century, temperature changes under RCP4.5 in both regions level off, following GHG concentrations. The contrast between the temperature changes in RCP4.5 and RCP8.5 demonstrate that the temperature change under RCP8.5 is due primarily to GHG increases.

4. Trends in Jet Position

[17] Figure 2 showed trends in both the extratropical and subtropical components of the Austral jet. In this study the focus is on the extratropical jet, defined here as the first local maximum in zonal-mean zonal-wind at 500 hPa

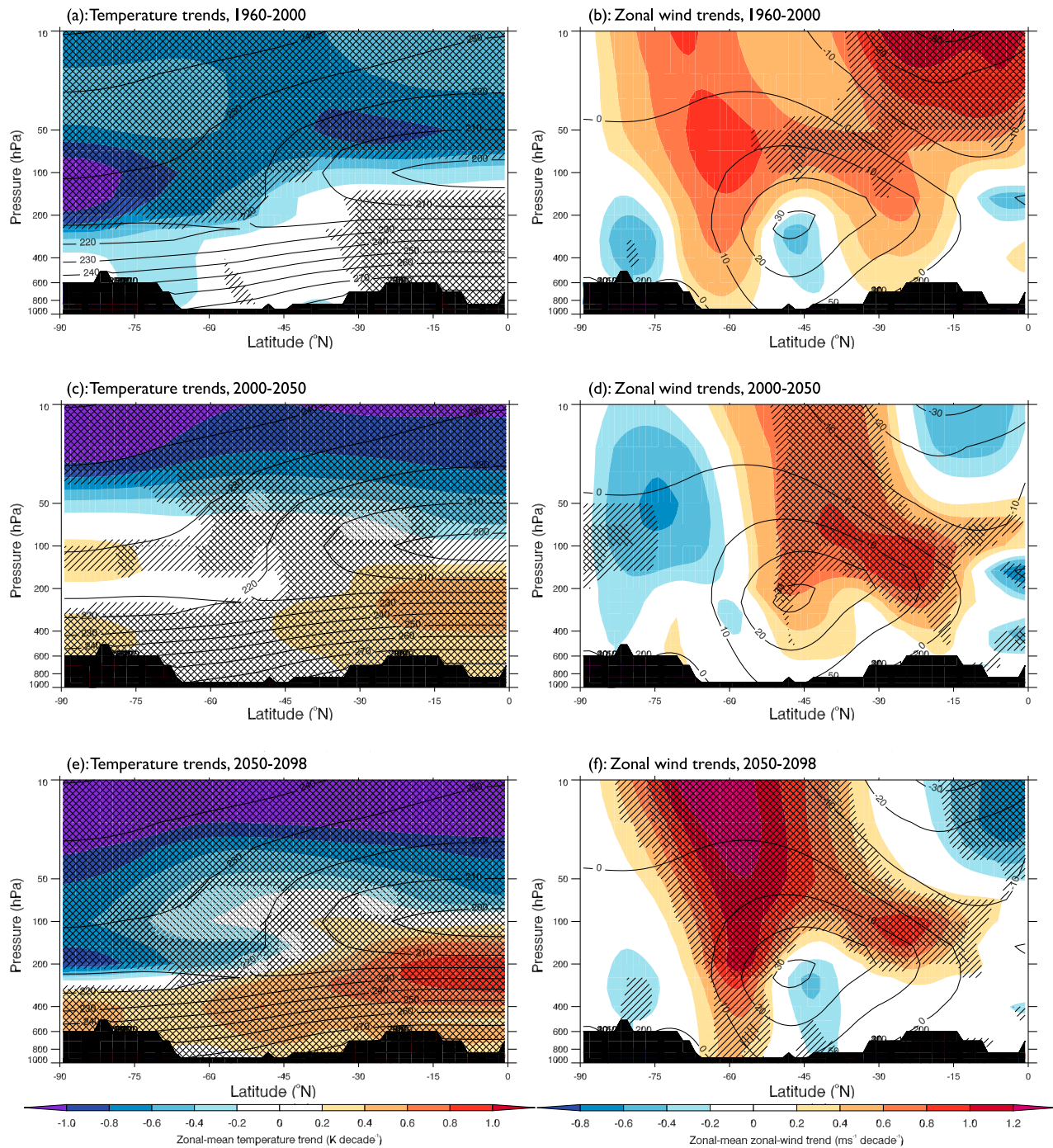


Figure 2. DJF zonal-mean (left) temperature (K) and (right) zonal-mean zonal-wind (ms^{-1}) from HadGEM2-ES. Colors show the linear trend (K/decade and $\text{ms}^{-1}/\text{decade}$) for (a and b) 1960–2000, (c and d) 2000–2050, and (e and f) 2050–2098, based on the historical and RCP8.5 experiments. Contours show the 1860–1900 mean. Hatching indicates a significant difference from zero, using a 2-tailed t-test, at the 5% level. Cross-hatching indicates significance at the 1% level.

equatorward of 65°S where the zonal-mean wind speed is greater than 10 m s^{-1} . Data are provided on a range of horizontal grids (Table 1). To locate the jet, zonal-mean monthly mean data are first linearly interpolated onto a 0.5° latitude grid. Local maxima are then identified using the first derivative of zonal-mean wind with respect to latitude. On the rare occasions when no local maxima can be

identified between 65°S and 25°S , jet position is defined as the position of the minimum in the second derivative of zonal-mean monthly mean zonal-wind within this latitude range.

[18] Figure 3b shows that the mean position of the jet is more equatorward in the high-top models, compared to the low-top models. The high-top jet moves poleward more

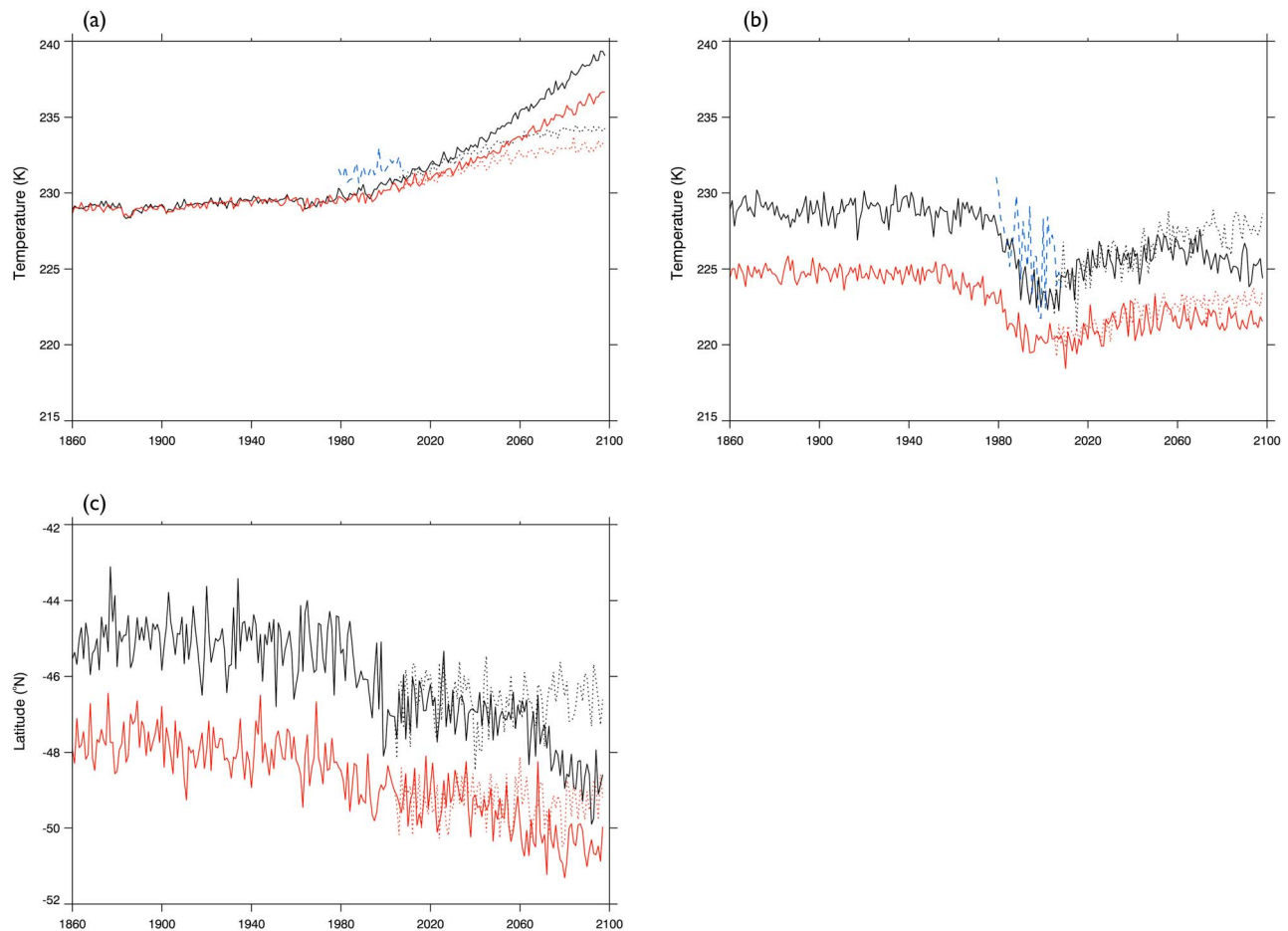


Figure 3. (a) DJF mean temperature (K) at 250 hPa, 0–25°S (tropical upper-troposphere), (b) DJF mean temperature (K) at 150 hPa, 75–90°S (polar lower-stratosphere), and (c) DJF mean jet latitude (°N). Solid lines show the historical (1850–2005) and RCP8.5 (2006–2098) experiments, and dotted lines show the historical and RCP4.5 experiments for the high-top (black) and low-top (red) ensemble mean. ERA-Interim values are shown in blue (Figures 3a and 3b only).

rapidly, especially under RCP8.5, and the difference between the position of the high- and low-top jets decreases with time. A decrease in the rate of change in the position of the jet is seen in both ensemble means and forcing scenarios in the first half of the 21st century, although it is more pronounced and more persistent in the high-top ensemble. There is a suggestion of a brief reversal of the trend in the high-top mean from 2000–2020. The jet then resumes its poleward migration under RCP8.5, with the high-top jet again moving more rapidly than the low-top. Jet position remains almost constant in the latter half of the 21st century under RCP4.5.

[19] Examination of the 1979–2006 zonal-mean zonal winds showed that the latitude of the DJF jet in the CMIP5 models was generally too far equatorward compared to reanalyses (Figure 4). The mean latitude of the jet at 500 hPa is 46°S and 49°S in the high- and low-top models respectively. The mean latitude of the ERA-Interim and CFSR jets is 49°S, compared to 50°S in NCEP/NCAR. Mean jet latitudes in the individual models lie in the range 52°S (CCSM4) to 43°S (IPSL-CM5A-LR), with high-top models tending to have more equatorward jets (Figure 4).

[20] Linear least-squares trends (DJF, 1979–2006) in jet position are -0.51 , -0.49 , and $-1.07^\circ\text{N}/\text{decade}$ in ERA-Interim, CFSR, and NCEP/NCAR respectively, giving a reanalysis mean trend of $-0.69 \pm 0.30^\circ\text{N}/\text{decade}$. The CMIP5 multimodel mean is in good agreement with the reanalyses for this period: $-0.60 \pm 0.28^\circ\text{N}/\text{decade}$. The high-top models overestimate the trend ($-0.94 \pm 0.25^\circ\text{N}/\text{decade}$), while the low-top models underestimate the trend ($-0.27 \pm 0.12^\circ\text{N}/\text{decade}$). Two low-top models give slightly positive (equatorward) trends for this period in response to recovering stratospheric ozone concentrations, contributing to the underestimate of the trends in the low-top mean.

[21] None of the CMIP5 models considered here simulate a jet shift of more than 5° poleward of their 1860–1900 position by 2098 under the high forcing RCP8.5 scenario.

4.1. Temperature Trends as a Driver for Jet Changes

[22] Changes in the position of the extratropical jet are linked to changes in the meridional temperature gradient [Lee and Kim, 2003]. This relationship can be seen in

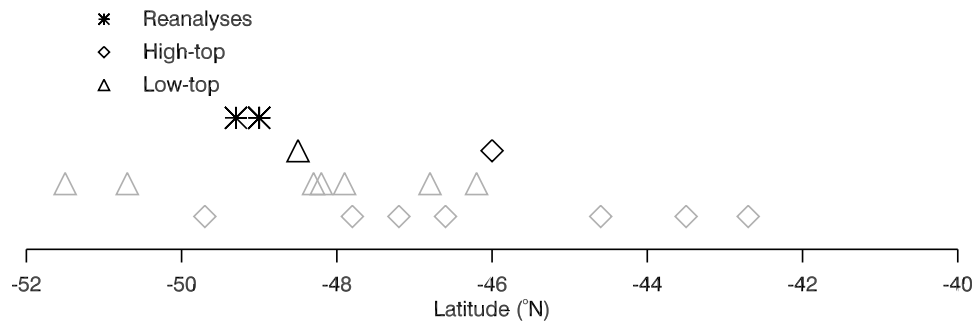


Figure 4. DJF (1979–2006) mean 500 hPa jet position from ERA-Interim, CFSR, and NCEP/NCAR, the high- and low-top multimodel means, and the individual CMIP5 models considered.

Figure 5. Figure 5a shows the trend in jet position and meridional temperature gradient, under RCP8.5, for each model for 1960–2000 (black), 2000–2050 (blue) and 2050–2098 (red). Figure 5b shows the high- and low-top multimodel mean. Here, the meridional temperature gradient is defined as the difference between polar average lower-stratospheric temperature (150 hPa, 75–90°S) and tropical upper-tropospheric temperature (250 hPa, 0–25°S) (as shown in Figure 3).

[23] Figure 5a shows a largely compact linear relationship (discussed further in section 4.2) between meridional temperature gradient and jet shift. A least-squares fit for 1960–2000, when the linear relationship is strongest, shows that a temperature trend of +1 K/decade typically results in a poleward jet shift of $\frac{1}{3}$ °S. This relationship becomes slightly less well defined in future as the model spread increases.

[24] Figure 5b shows low- and high-top ensemble mean trends. The trend in meridional temperature gradient is larger in the high-top models (Figure 5b). The high-top and low-top values are significantly different at the 5% level (‘separable’) in all periods considered. Warming of the polar lower-stratosphere in the period 2000–2050 results in a near zero trend in both high- and low-top meridional temperature gradient.

[25] High-top models have a larger jet shift in 1960–2000 (Figure 5, black) and 2050–2098 (red), compared to the low-tops, as a result of the larger temperature trends. Variability in jet position is greater than that in temperature, so confidence intervals are larger, but jet responses are separable in 2050–2098 (red, Figure 5b). The mean position trend for 2050–2098 in high-top models is -0.59 °N/decade compared to -0.21 °N/decade for the low-top models. In 2000–2050 the magnitude of the jet shift is not significantly different from zero at the 5% level in either ensemble mean (Figure 5b). Small or zero trends in jet position in this period are the result of a near cancellation between the effects of increasing GHG and stratospheric ozone concentrations. Such a cancellation was also highlighted by *Polvani et al.* [2011].

[26] Detailed examination of the mechanisms that drive changes in the position of the jets is beyond the scope of this study. There is a developing consensus in the literature that the changes are linked to the impact of the upper level pole-to-equator temperature gradient and the linked stratospheric wind shear on the type of non-linear wave-breaking in the troposphere [*Wittman et al.*, 2007]. Increases in the pole-to-equator temperature gradient lead to increases in upper level baroclinicity and an increase in anticyclonic LC1 type wave-breaking linked to a shift in the mean eddy length scales

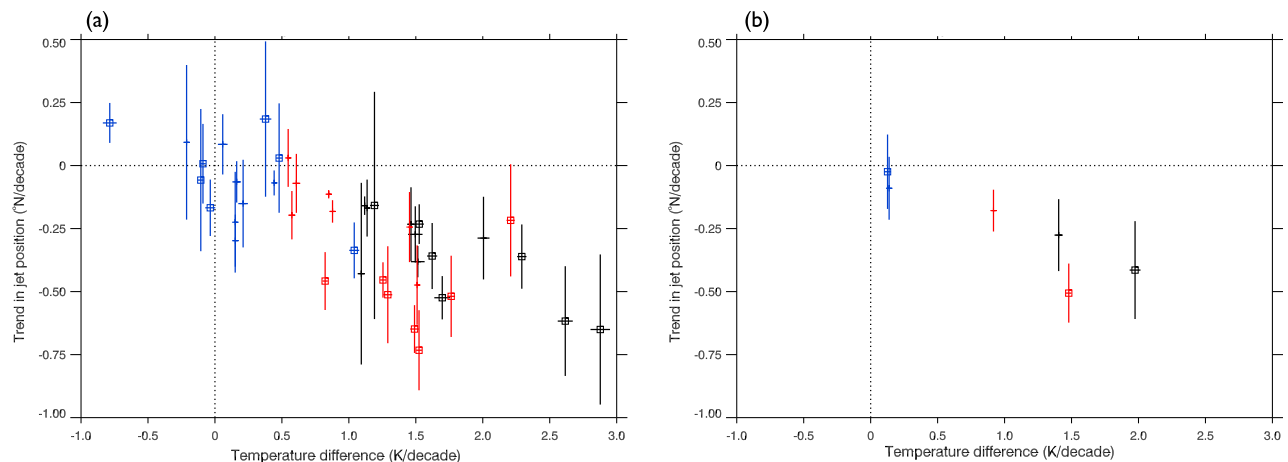


Figure 5. (a) Meridional temperature gradient (K/decade) and 500 hPa jet position (°N/decade) trends for each model for 1960–2000 (black), 2000–2050 (blue), and 2050–2098 (red) for RCP8.5. Squares indicate high-top models. Error bars for individual models are one standard error. (b) Same as Figure 5a but for the low- and high-top multimodel mean. Error bars for multimodel means are two standard errors.

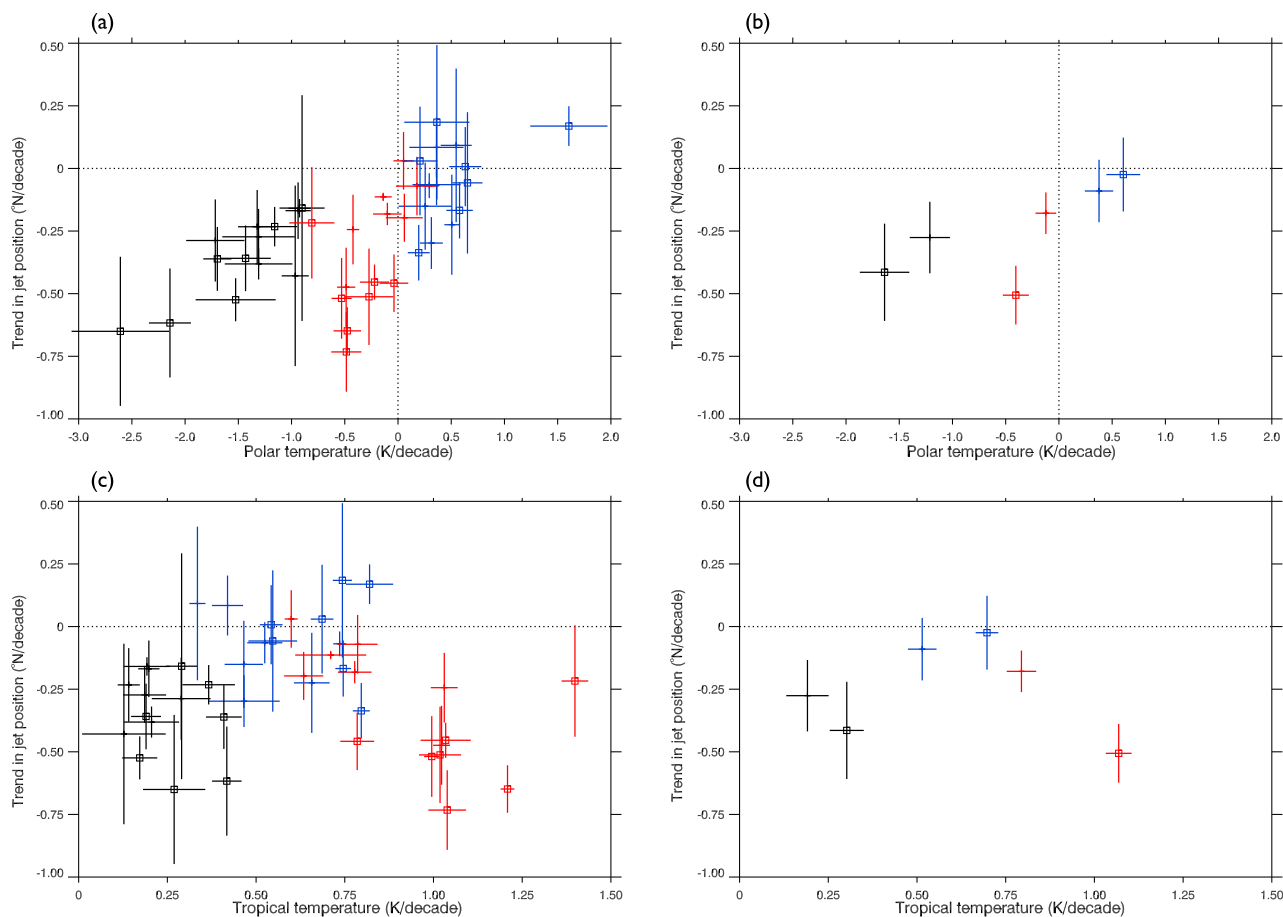


Figure 6. (a) Polar lower-stratospheric temperature (K/decade) and 500 hPa jet position ($^{\circ}$ N/decade) trends for each model for 1960–2000 (black), 2000–2050 (blue), and 2050–2098 (red) for RCP8.5. (b) Same as Figure 6a but for the low- and high-top multimodel mean. (c) Tropical upper tropospheric temperature (K/decade) and jet position ($^{\circ}$ N/decade) trends for each model. (d) Same as Figure 6c but for the low- and high-top multimodel mean. Squares indicate high-top models. Error bars for individual models (Figures 6a and 6c) are one standard error. Error bars for multimodel means (Figures 6b and 6d) are two standard errors.

toward longer wavelengths [Riviere, 2011]. As shown by McLandress *et al.* [2011b], this mechanism is consistent with the observed poleward shift in momentum flux convergence on the poleward side of the eddy driven jet. The recent analyses of Wang and Magnusdottir [2011] and Ndarana *et al.* [2012] both point to a large increase in anticyclonic wave-breaking on the equatorward side of the SH jet, consistent both with this picture and the observed poleward shift of the jet.

[27] Meridional temperature gradient has been defined in this study as the difference between the polar average lower-stratospheric temperature and tropical upper-tropospheric temperature. To understand further the origin of the changes in meridional temperature gradient, the contribution to the gradient trend from each of these regions is shown in Figure 6, plotted against the total jet shift, as in Figure 5.

[28] Figure 6a shows polar lower-stratospheric temperature trends for each model for 1960–2000 (black), 2000–2050 (blue), and 2050–2098 (red). Polar lower stratospheric temperature trends are negative in all models for 1960–2000, ranging from -2.61 K/decade in GFDL-CM3 to -0.90

K/decade in HadGEM2-CC (the latter is not significantly different from zero at the 5% level). The multimodel means (Figure 6b) show greater lower-stratospheric cooling trends in high-top models compared to low-top models in 1960–2000 (black) and 2050–2098 (red): -1.64 K/decade compared to -1.40 K/decade for 1960–2000 and -0.41 K/decade compared to -0.12 K/decade for 2050–2098. Estimates from the two sets of models are separable in both periods. Opposite temperature trends in the region of $+0.5$ K/decade are found across all models during 2000–2050 (blue).

[29] In 2000–2050 stratospheric ozone recovery typically dominates the polar temperature trend, and all models predict a warming trend there. In this period, low-top models predict a warming of 0.38 K/decade, while high-top models predict a larger trend of $+0.61$ K/decade (Figure 6b). However, the trends from high- and low-top models are not separable. Some models predict an equatorward trend in jet position in this period, although only the GFDL-CM3 trend is significantly different from zero at the 5% level.

[30] Figure 6c shows tropical upper-tropospheric temperature trends, plotted against the trend in jet position.

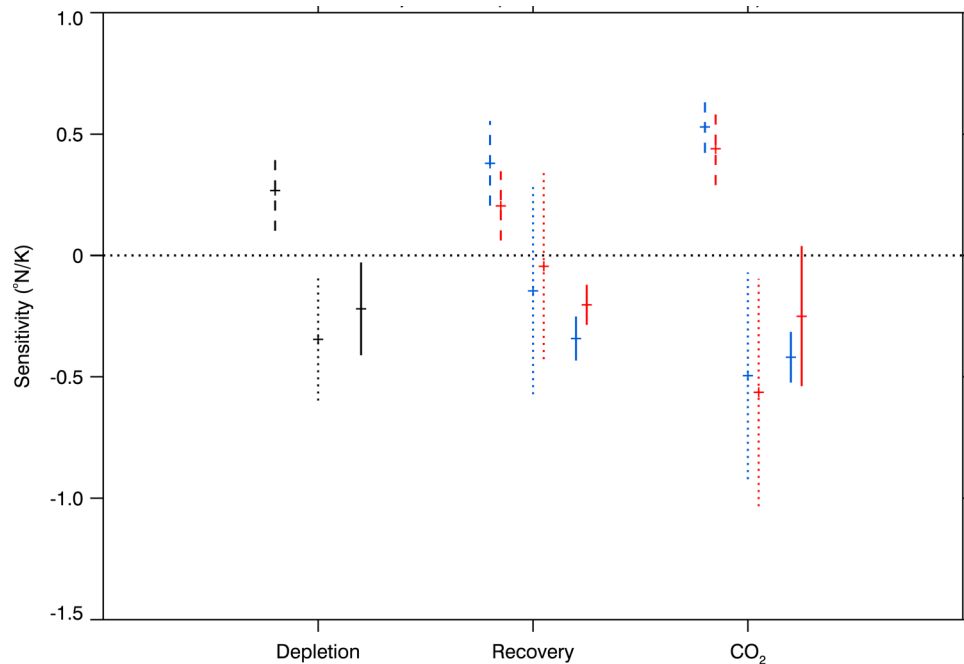


Figure 7. Sensitivity ($^{\circ}\text{N}/\text{K}$) of the position of the 500 hPa jet to trends in polar lower-stratosphere temperature (dashed), tropical upper-troposphere temperature (dotted), and meridional temperature gradient (solid), in the ozone depletion (1960–2000), ozone recovery (2000–2050), and GHG dominated (2050–2098) periods. Historical data are shown in black, RCP4.5 in blue, and RCP8.5 in red. Error bars are two standard errors.

The high- and low-top multimodel means are shown in Figure 6d. All models have warming trends in all periods. The magnitude of the trends increases with time, as expected from the increasing GHG concentration gradients shown in Figure 1, and the tropical temperature response shown in Figure 3a. Multimodel means (Figure 6d) show larger temperature trends in the high-top models compared to the low-top models. The trends are separable in each period, and the difference between them increases with time. The difference between the warming trends in the high- and low-top models is especially pronounced in 2050–2098, with a mean trend of $+1.07$ K/decade predicted in the high-top models, compared to $+0.79$ K/decade in the low-top models.

[31] Enhanced warming in the tropical upper-troposphere in the high-top models compared to the low-tops could be the result of differing parameterizations of moist processes, different tropical tropopause layer processes, or differences in stratospheric upwelling. The very limited number of direct, single model, high- and low-top comparisons available in CMIP5 make it difficult to determine whether the representation of the stratosphere plays an important role in this difference without further experiment.

4.2. Linearity in the Jet Response to Temperature Trends

[32] The mean ratio of trends in jet position to trends in temperature gives a measure of the sensitivity of the jet response to the temperature trend. The sensitivity of jet position trends to meridional temperature gradient trends, and polar and tropical temperature trends, is shown in Figure 7 for RCP8.5 (red) and RCP4.5 (blue). Negative

sensitivity indicates a poleward movement in response to positive temperature trends, positive sensitivity indicates a poleward movement in response to negative temperature trends.

[33] The sensitivity of the jet to each of the three temperature trends is invariant across all the time periods and forcing scenarios considered. The sensitivity of the jet to meridional temperature gradient changes (solid lines) remains in the region of $-0.3^{\circ}\text{N}/\text{K}$ across all periods, and both forcing scenarios. However, there are larger error bars in 2050–2098 in the RCP8.5 case. The sensitivity of the jet to polar lower-stratospheric temperature trends is $0.4^{\circ}\text{N}/\text{K}$, with no significant differences between the two forcing scenarios considered.

[34] The relationship between tropical upper-tropospheric temperature trends and jet position trends is weaker than those in the temperature gradient and polar lower-stratospheric temperature cases, and the errors intersect zero in the 2000–2050 case under both RCP4.5 and RCP8.5 (Figure 7). However, there is insufficient evidence to suggest that the sensitivity of the jet to tropical upper-tropospheric temperature trends changes with forcing.

[35] Analysis of the latitude of jet in the individual models considered showed a decrease in the rate of change of jet position in some individual models, and also in the low-top mean, after 2080 in the RCP8.5 scenario (Figure 3c). This change was apparent in IPSL-CM5A, HadGEM2-CC, Nor-ESM1-M, and CSIRO-Mk3.6, hinting at a possible deviation from a linear jet response to temperature trends in these models. However, this change can only be seen over a short

Table 2. Correlation Between Jet Position and Shift

	SON	DJF	MAM	JJA	Ann
KG	−0.61	−0.08	−0.76	−0.81	−0.77
This work	−0.30	−0.37	−0.74	−0.53	−0.64

period. As such, it cannot be demonstrated to be significantly different to the 50-year trends considered in Figure 7.

[36] A decrease in the rate of change of jet position as the jets are located closer to the pole would be consistent with the findings of *Barnes and Hartmann* [2010]. They suggest that the jet shift lessens as it moves poleward because the positive feedback between eddies and the mean flow is reduced due to the inhibition of polar wave-breaking for jets positioned at high latitudes. Despite some evidence in time series from individual models, there is no clear evidence of an approach to a geometric limit on the absolute shift of the jet in the ensemble mean by the end of the 21st century, even under the large forcing RCP8.5 scenario.

5. The Relationship Between Jet Latitude and Jet Shift

[37] Related to the results of *Barnes and Hartmann* [2010], *Kidston and Gerber* [2010] (hereafter, KG10) found the magnitude of the poleward jet shift in CMIP3 models to be well correlated with biases in the initial position of the jet in 20th century simulations. Equatorward biases resulted in larger shifts. The strong correlation between the shift and initial latitude of the 10 m jet existed in all seasons except DJF. KG10 attributed the poor DJF correlation to the fact that not all CMIP3 models included ozone changes, resulting in very different forcings across the models. This is not a factor in the analysis of CMIP5 models due to the use of a consistent ozone database.

[38] All of the CMIP3 models used by KG10 had climatological jets (in the annual mean for 1960–2000) that were too far equatorward compared to the NCEP/NCAR reanalysis. In section 4, CMIP5 models were shown to have DJF jet latitudes equatorward of those from reanalyses. This is also true for the annual mean multimodel mean (1979–2006). Jet positions in individual models range from 42°S (IPSL-CM5A-LR) to 52°S (CCSM4), with a low-top mean of 48°S, and a high-top mean of 46°S. The ERA-Interim and CFSR jets in this period are found at 50°S, and the NCEP/NCAR jet is at 53°S.

[39] Repeating the experiment described by KG10 using our 500 hPa jet, and determining the absolute shift in the jet between 1960–2000 and 2060–2098 under the RCP8.5 scenario, we find a weaker relationship than KG10 between annual mean shift and 1960–2000 position (Table 2). A weaker correlation compared to the KG10 result is also found in SON and JJA. A stronger correlation is seen in DJF, which is to be expected due to the consistent representation of ozone in CMIP5 models. However, this relationship is still weak, with $r = -0.37$. The only significant relationship found here ($r = -0.74$) is in MAM.

[40] Overall, the relationship between initial jet position and the magnitude of the jet shift was found to be weaker in

this subset of CMIP5 models, compared to the relationship identified by KG10.

6. Conclusions and Discussion

[41] The analysis here has shown that high-top models have larger temperature and jet position responses to forcing compared to low-top models. These models have historical polar lower-stratospheric temperatures and tropical upper-tropospheric temperatures in better agreement with reanalyses (Figure 3a). High-top models gave overestimates of the 1979–2006 trend in jet position relative to the reanalyses, while the low-top ensemble underestimated the trend. Overall, the subset of CMIP5 models used in this work gave a good representation of the 1979–2006 trend in jet position.

[42] A systematic relationship has been identified between the trend in jet position and the trend in polar lower-stratospheric temperature, tropical upper-tropospheric temperature, and, in particular, meridional temperature gradient. Increases in upper-level meridional temperature gradient cause a poleward movement of the jet. Such increases occur in 1960–2000, primarily as a result of stratospheric ozone depletion and the associated cooling of the polar lower-stratosphere, and in 2050–2098, primarily a result tropical upper-tropospheric warming due to GHG increases. Cancellation between the effects of increasing stratospheric ozone and GHG concentrations are apparent in 2000–2050, especially in the high-top models (Figure 5).

[43] Jet responses from the high- and low-top ensemble are separable in DJF 2050–2098 under RCP8.5. High-top models predict an ensemble mean trend of $-0.51 \pm 0.08^\circ\text{N}$, more than double the low-top trend (Figure 5b). Meridional temperature gradient trends from the high-top ensemble are approximately double those from the low-top ensemble for 1960–2000 and 2050–2098 (Figure 5b). For 1960–2000, this difference is the result of a combination of enhanced warming in the tropical upper-troposphere and enhanced cooling of the polar lower-stratosphere in the high-top models. In 2050–2098 the difference between high- and low-top meridional temperature gradient trends is primarily the result of enhanced tropical upper-tropospheric warming in the high-top models (Figure 6). Jet position and meridional temperature gradient responses for 2000–2050 are not significantly different between the two sets of models, though there is still clear enhancement of tropical upper-tropospheric temperature trends in the high-top ensemble. A similar pattern of responses exists under RCP4.5, but many of the changes that occur in this scenario are very close to zero, and it is not possible to separate the two sets of models.

[44] Previous studies have linked absolute jet shift to initial jet position. This relationship was found in this subset of CMIP5 models for some seasons, but was not as strong as has been identified in previous studies (Table 2). In DJF, the main focus of this study, the magnitude of the jet shift was found to be independent of the initial latitude of the jet. It has also been suggested in previous work that the jet position response to temperature trends is non-linear. No evidence was found in this subset of models to suggest that there is a significant deviation from a linear response of jet position to trends in meridional temperature gradient. Analyses of the sensitivity of the position of the jet to meridional temperature gradient, polar lower-stratospheric temperature, and

tropical upper-tropospheric temperature all showed a linear response, i.e. there was no change in the sensitivity of jet position to temperature trends for changes in forcing (Figure 7).

[45] Changes in Austral jet position are related to changes in precipitation patterns [Gillet *et al.*, 2006], Antarctic sea ice extent [Stammerjohn *et al.*, 2008], and carbon uptake by the Southern Ocean [Lovenduski *et al.*, 2007]. Hence, realistic predictions of trends in the position of the Austral jet, and an understanding of the mechanisms behind such trends, are important. As the sensitivity of the trend in jet position to temperature trends is robust, a key to improved estimates of future jet position is improved estimates of temperature trends. The results of this work suggest that a full representation of the stratosphere in models may be important for such improvements.

[46] **Acknowledgments.** This work was funded by the National Centre for Atmospheric Science (NCAS)-Climate via a CMIP5 grant. We acknowledge the World Climate Research Programme's Working Group on Coupled Modeling, which is responsible for CMIP, and we thank the climate modeling groups for producing and making available the model output listed in Table 1. For CMIP the U.S. Department of Energy's Program for Climate Model Diagnosis and Intercomparison provides co-ordinating support and led development of software infrastructure in partnership with the Global Organization for Earth System Science Portals. We also thank the British Atmospheric Data Centre (BADC) for providing access to their CMIP5 data archive, and acknowledge the use of ERA data made available by the BADC and NCAS-Climate. NCEP/NCAR data was provided by NOAA/OAR/ESRL PSD, and CFSR data was provided by NCAR, via the Research Data Archive (RDA).

References

- Arblaster, J. M., and G. A. Meehl (2006), Contributions of external forcings to Southern Annular Mode trends, *J. Clim.*, *19*, 2896–2905, doi:10.1175/JCLI3774.1.
- Archer, C. L., and K. Caldeira (2008), Historical trends in the jet streams, *Geophys. Res. Lett.*, *35*, L08803, doi:10.1029/2008GL033614.
- Barnes, E. A., and D. L. Hartmann (2010), Testing a theory for the effect of latitude on the persistence of eddy-driven jets using CMIP3 simulations, *Geophys. Res. Lett.*, *37*, L15801, doi:10.1029/2010GL044144.
- Cionni, I., et al. (2011), Ozone database in support of CMIP5 simulations: Results and corresponding radiative forcing, *Atmos. Chem. Phys. Discuss.*, *11*, 10,875–10,933, doi:10.5194/acpd-11-10875-2011.
- Cordero, E. C., and P. M. D. F. Forster (2006), Stratospheric variability and trends in models used for the IPCC AR4, *Atmos. Chem. Phys.*, *6*(12), 5369–5380.
- Dee, D. P., et al. (2011), The ERA-Interim reanalysis: Configuration and performance of the data assimilation system, *Q. J. R. Meteorol. Soc.*, *137*(656), 553–597, doi:10.1002/qj.828.
- Fu, Q., and P. Lin (2011), Poleward shift of subtropical jets inferred from satellite-observed lower-stratospheric temperatures, *J. Clim.*, *24*, 5597–5603, doi:10.1175/JCLI-D-11-00027.1.
- Gillet, N. P., T. D. Kell, and P. D. Jones (2006), Regional climate impacts of the Southern Annular Mode, *Geophys. Res. Lett.*, *33*, L23704, doi:10.1029/2006GL027721.
- Hudson, R. D. (2011), Measurements of the movement of the jet streams at mid-latitudes, in the Northern and Southern Hemispheres, 1979 to 2010, *Atmos. Chem. Phys. Discuss.*, *11*, 31,067–31,090.
- Kalnay, E., et al. (1996), The NCEP/NCAR 40-year reanalysis project, *Bull. Am. Meteorol. Soc.*, *77*(3), 437–471, doi:10.1175/1520-0477(1996)077<0437:TNYRP>2.0.CO;2.
- Kidston, J., and E. P. Gerber (2010), Intermodel variability of the poleward shift of the austral jet stream in the CMIP3 integrations linked to biases in 20th century climatology, *Geophys. Res. Lett.*, *37*, L09708, doi:10.1029/2010GL042873.
- Lee, S., and H.-K. Kim (2003), The dynamical relationship between subtropical and eddy-driven jets, *J. Atmos. Sci.*, *60*, 1490–1503, doi:10.1175/1520-0469(2003)060<1490:TDRBSA>2.0.CO;2.
- Lovenduski, N. S., N. Gruber, S. C. Doney, and I. D. Lima (2007), Enhanced CO₂ outgassing in the Southern Ocean from a positive phase of the Southern Annular Mode, *Global Biogeochem. Cycles*, *21*, GB2026, doi:10.1029/2006GB002900.
- Marshall, G. J. (2003), Trends in the Southern Annular Mode from observations and reanalyses, *J. Clim.*, *16*, 4134–4143, doi:10.1175/1520-0442(2003)016%3C4134%3ATITSAM%3E2.0.CO%3B2.
- McLandress, C., J. Perlwitz, and T. G. Shepherd (2011a), Comment on “tropospheric temperature response to stratospheric ozone recovery in the 21st century” by Hu *et al.* (2011), *Atmos. Chem. Phys. Discuss.*, *11*, 32,993–33,012, doi:10.5194/acpd-12-2853-2012.
- McLandress, C., T. G. Shepherd, J. F. Scinocca, D. A. Plummer, M. Sigmund, A. I. Jonsson, and M. C. Reader (2011b), Separating the dynamical effects of climate change and ozone depletion. Part II: Southern Hemisphere troposphere, *J. Clim.*, *24*(6), 1850–1868, doi:10.1175/2010JCLI3958.1.
- Ndarana, T., D. W. Waugh, L. M. Polvani, G. J. P. Correa, and E. P. Gerber (2012), Antarctic ozone depletion and trends in tropopause Rossby wave breaking, *Atmos. Sci. Lett.*, doi:10.1002/asl.384, in press.
- Polvani, L. M., M. Previdi, and C. Deser (2011), Large cancellation, due to ozone recovery, of future Southern Hemisphere atmospheric circulation trends, *Geophys. Res. Lett.*, *38*, L04707, doi:10.1029/2011GL046712.
- Riahi, K., et al. (2011), RCP 8.5—A scenario of comparatively high greenhouse gas emissions, *Clim. Change*, *109*, 33–57, doi:10.1007/s10584-011-0149-y.
- Riviere, G. (2011), A dynamical interpretation of the poleward shift of the jet streams in global warming scenarios, *J. Atmos. Sci.*, *68*, 1253–1272, doi:10.1175/2011JAS3641.1.
- Saha, S., et al. (2010), The NCEP climate forecast system reanalysis, *Bull. Am. Meteorol. Soc.*, *91*, 1015–1057, doi:10.1175/2010BAMS3001.1.
- Seidel, D. J., Q. Fu, W. J. Randel, and T. J. Reichler (2008), Widening of the tropical belt in a changing climate, *Nat. Geosci.*, *1*, 21–24, doi:10.1038/ngeo.2007.38.
- Son, S.-W., et al. (2008), The impact of stratospheric ozone recovery on the Southern Hemisphere westerly jet, *Science*, *320*(5882), 1486–1489, doi:10.1126/science.1155939.
- Stammerjohn, S. E., D. G. Martinson, R. C. Smith, X. Yuan, and D. Rind (2008), Trends in Antarctic annual sea ice retreat and advance and their relation to El Niño–Southern Oscillation and Southern Annular Mode variability, *J. Geophys. Res.*, *113*, C03S90, doi:10.1029/2007JC004269.
- Thompson, D. W. J., and S. Solomon (2002), Interpretation of recent Southern Hemisphere climate change, *Science*, *296*(5569), 895–899, doi:10.1126/science.1069270.
- Thomson, A., et al. (2011), RCP4.5: A pathway for stabilization of radiative forcing by 2100, *Clim. Change*, *109*, 77–94, doi:10.1007/s10584-011-0151-4.
- Wang, Y.-H., and G. Magnusdottir (2011), Tropospheric Rossby wave breaking and the SAM, *J. Clim.*, *24*, 2134–2146, doi:10.1175/2010JCLI4009.1.
- Wittman, M. A. H., A. J. Charlton, and L. M. Polvani (2007), The effect of lower stratospheric shear on baroclinic instability, *J. Atmos. Sci.*, *64*, 479–496, doi:10.1175/JAS3828.1.